Nanoscale

COMMUNICATION

View Article Online
View Journal | View Issue

Cite this: *Nanoscale*, 2014, **6**, 4555

Received 24th December 2013
Accepted 6th February 2014

DOI: 10.1039/c3nr06810b

www.rsc.org/nanoscale

A solar-thermal energy harvesting scheme: enhanced heat capacity of molten HITEC salt mixed with Sn/SiO_x core–shell nanoparticles†

Chih-Chung Lai,[a] Wen-Chih Chang,[a] Wen-Liang Hu,[b] Zhiming M. Wang,[c] Ming-Chang Lu*[b] and Yu-Lun Chueh*[a]

We demonstrated enhanced solar-thermal storage by releasing the latent heat of Sn/SiO_x core–shell nanoparticles (NPs) embedded in a eutectic salt. The microstructures and chemical compositions of Sn/SiO_x core–shell NPs were characterized. *In situ* heating XRD provides dynamic crystalline information about the Sn/SiO_x core–shell NPs during cyclic heating processes. The latent heat of ~29 J g^{-1} for Sn/SiO_x core–shell NPs was measured, and 30% enhanced heat capacity was achieved from 1.57 to 2.03 J g^{-1} K^{-1} for the HITEC solar salt without and with, respectively, a mixture of 5% Sn/SiO_x core–shell NPs. In addition, an endurance cycle test was performed to prove a stable operation in practical applications. The approach provides a method to enhance energy storage in solar-thermal power plants.

1. Introduction

Recently, renewable energies, such as wind,[1] hydroelectricity,[2] and solar energy,[3] have attracted significant attention due to the limited availability of fossil fuels and global concerns of climate change. Among all the renewable energies, solar energy is the most promising energy-harvesting resource because of its abundance. For example, the amount of daily solar irradiation on the earth's surface is enough to satisfy global annual energy consumption.[4] Photovoltaics (PVs), which directly convert solar energy into electricity, suffer from low energy conversion efficiency[5] (<20% for Si-based modules) and the limitation of the diurnal nature of solar power. On the other hand, solar-thermal power generation, which stores sunlight as heat and converts it into electricity when power is needed, could offer a much higher efficiency[6] (*e.g.*, approximately 40%) and also overcome the diurnal limitation of solar power.

A schematic of a solar-thermal power plant is shown in Fig. 1. The solar-thermal power plant includes an array of heliostats, which reflect and concentrate sunlight continuously toward the tower receiver where the molten salt is heated. The hot molten salt flows to a hot storage tank for thermal energy storage. When power is needed, the hot molten salt is transported to a heat exchanger, boiling water into steam to activate the turbine. The mechanical work of the turbine is then converted into electricity by a generator. The cooled molted salt, which has exhausted its thermal energy, flows to a cold storage tank to complete a cycle.[7] The amount of power generation in the solar-thermal system is limited by the amount of thermal energy stored, which is determined by the heat capacity (HC) of the working fluid in the solar-thermal power plants. Molten salts, which are currently used as the working fluids in the

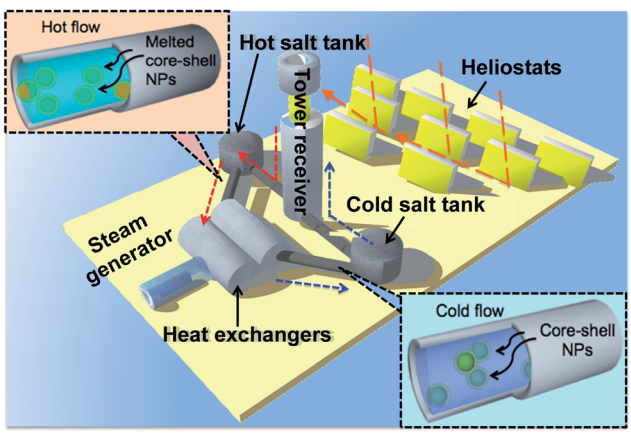

Fig. 1 Schematic of Sn/SiO_x core–shell NPs mixed with molten salt for the thermal power plant.

[a]*Department of Materials Science and Engineering, National Tsing Hua University, Hsinchu, 30013, Taiwan. E-mail: ylchueh@mx.nthu.edu.tw*

[b]*Department of Mechanical Engineering, National Chiao Tung University, Hsinchu, 30013, Taiwan. E-mail: mclu@mail.nctu.edu.tw*

[c]*State Key Laboratory of Electronic Thin Films and Integrated Devices University of Electronic Science and Technology of China, Chengdu 610054, P. R. China*

† Electronic supplementary information (ESI) available: Detailed experimental results are included for the following: SEM images of the HITEC molten salt with and without a mixture of Sn/SiO_x core–shell NPs; statistical diameter distribution of pure Sn and Sn/SiO_x core–shell NPs; the HAADF image and EDS linescan profile of a Sn/SiO_x core–shell NP; XRD analysis for Sn NPs annealing at different heating temperatures; the XRD spectra of Sn/SiO_x core–shell NPs before and after RTA for the shell protection test. See DOI: 10.1039/c3nr06810b

power plants, have a relatively low specific heat of approximately 1.5 kJ kg^{-1} K^{-1} (ref. 8) compared to that of liquid water (4 kJ kg^{-1} K^{-1}). Although, the wide operation temperature region of molten salts makes it better as a flowing energy-storage medium compared to liquid water, the inferior thermal property of molten salts limits the energy storage capacity and consequently impedes the applications of power plants.

Enhancement of thermal energy storage by using the latent heat of materials has recently been proposed and demonstrated. For example, the employment of phase change materials (PCMs) in heat exchangers to enhance the thermal energy storage has been demonstrated. However, the low thermal conductivity of PCMs limits the efficiency of solar-thermal plants.[9–11] Although the improvement of heat transfer for the PCMs has been shown by inserting metallic fillers, metal matrix structures, finned tubes or aluminum shavings, these approaches lead to rather complex systems, and the inserted composite materials remain an issue for cyclic-operations.[12] Core–shell micro-particles have been applied to enhance thermal storage of the working fluids by using the latent heat of the particles. However, the low thermal conductivity of the paraffin-based microparticles,[13] and the potential oxidation and chemical reaction of the particles with eutectic salts at a high temperature, restrict their practical applications. Therefore, the selection and development of a proper core material with higher latent heat and a well-protected shell layer will be an important step in providing a stable core–shell NP of higher latent heat exhaustion in the operation temperature of certain eutectic salts. We selected tin as the core material because of both a high thermal conductivity of 66.8 W m^{-1} K^{-1} and a high latent heat of 7.03 kJ per mole. By introducing the concept of nanofluid,[14] the nano-sized additives can somehow enhance the heat transfer properties of eutectic salts without losing their viscosity. Toward this end, Sn/SiO_x core–shell nanoparticles (NPs) were synthesized and an enhanced HC of the molten salt was demonstrated by taking advantage of the large latent heat of the NPs. The concept demonstrated in this work provides a method to enhance solar-thermal power generation and could facilitate its application.

2. Experimental section

Fabrication of core–shell Sn/SiO_x nanoparticles

Tin (Sn) nanoparticles averaging 100 nm in diameter [Sigma Aldrich Co.] were used as a source of dispersed particles. A 0.05 M pre-treated solution was formed by stirring a mixture of Sn NPs with 50 ml ethanol. The solution was continuously stirred at a temperature of 80 °C. 50–100 μL of 97% 3-aminopropyl trimethoxysilane (APTMS) [Sigma Aldrich Co.] was then carefully dropped into the solution. Formation of the SiO_x shell layer was initiated by stirring the mixed solution at pH = 4–5. These pre-products were washed several times with ethanol solvent, followed by thermal annealing treatment for two hours.

Characterization

The phase and crystallinity of Sn NPs were characterized using an *in situ* X-ray diffractometer (XRD, Shimadzu XRD-6000) equipped with a vacuum-heating stage by using Cu Kα (λ = 0.154 nm) as the radiation source. The *in situ* XRD analyses of the core–shell systems were performed in a vacuum pressure of $\sim 10^{-3}$ Torr with a heating rate of 20 °C min^{-1} and cooling in air. Morphologies and microstructures were studied using a field-emission scanning electron microscope (FE-SEM, JSM-6500F, JEOL) and a transmission electron microscope (TEM, JEM-3000F, JEOL), equipped with an energy dispersive spectrometer (EDS). The thermal properties (latent heat and HC) of Sn NPs, Sn/SiO_x core–shell NPs, and HITEC salt mixed with different concentrations of Sn/SiO_x core–shell NPs were examined at a heating rate of 20 °C min^{-1} using a differential scanning calorimeter (DSC, DSC 1, METTLER TOLEDO).

3. Results and discussion

To achieve the enhanced HC of the molten salt by taking advantage of the large latent heat of the NPs, it is important to select a solar salt with a suitable working temperature range that fits the melting point of core–shell NPs. Three kinds of common molten salts, namely solar salt, HITEC, and HITEC XL, are listed in Table 1, which also provides the detailed chemical compositions, freezing temperature, melting temperature, and specific heat capacity. HITEC solar salt, composed of 7 wt% sodium nitrate ($NaNO_3$), 53 wt% potassium nitrate (KNO_3), and 40 wt% sodium nitrite ($NaNO_2$) with an operation temperature ranging from 142 to 535 °C,[15] was adopted as the representative molten salt to demonstrate the proposed concept. The scanning electron microscopy (SEM) images of the salt are shown in Fig. S1 in the ESI.† Tin (Sn) was chosen as the doping material, the latent heat of which can be contributed to heat storage at a melting temperature of 225 °C. To take advantage of the large latent heat of the Sn NPs while preventing oxidation and fusion with the existing molten salt during high temperature thermal cyclic processes, a SiO_x shell layer is synthesized on the surface of the Sn NP. Fig. 2 shows the schematics of the chemical method for Sn/SiO_x synthesis.[16,17] Sn NPs were first introduced into a precursor of 3-aminopropyl trimethoxysilane (APTMS) (CAS# 13822-56-5) with a pH value of 4–5 (see Methods for more details). By adjusting the amount of the precursor, the thickness of the SiO_x shell layer can be controlled. Subsequently, the pre-products were washed several times with ethanol solvent. These pre-products were then thermal annealed for two hours to obtain stable Sn/SiO_x core–shell NPs.

The SEM images of the Sn NPs are shown in Fig. 3(a). The NPs have an average diameter of approximately 110 nm as shown in Fig. S2, and the corresponding transmission electron microscopy (TEM) images of Sn NPs are shown in Fig. 3(b). The inset in Fig. 3(b) represents the selected area diffraction (SAD) pattern. The rings from the SAD pattern reveal a polycrystalline feature where the *d*-spacing with respect to each plane was indexed, confirming the configuration of Sn NPs. The SEM images of Sn/SiO_x NPs are shown in Fig. 3(c). After encapsulating the SiO_x layer on Sn NPs, no morphology change was found, as shown in the figure, whereas the average diameter of core–shell NPs increased to approximately 145 nm (see Fig. S2†). The TEM image shown in Fig. 3(d) indicates an

Table 1 Physical properties and compositions of different solar salts

Properties	Solar salt	HITEC	HITEC XL
$NaNO_3$	60%	7%	—
KNO_3	40%	53%	7%
$NaNO_2$	—	40%	45%
$Ca(NO_3)_2$	—	—	48%
Freezing point (°C)	220	142	120
Melting point (°C)	600	535	500
Heat capacity 300 °C, J g^{-1} K^{-1}	1.49	1.56	1.45

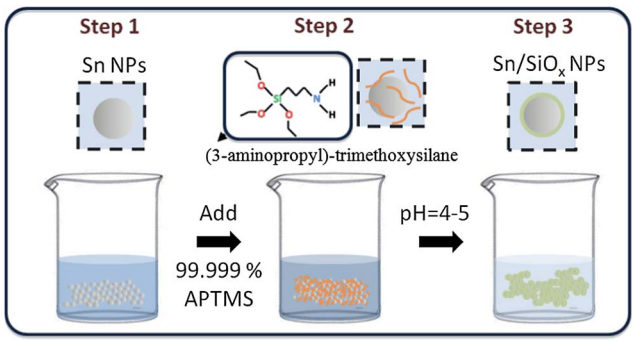

Fig. 2 Schematic of the formation of the SiO_x layer outside Sn NPs. (3-Aminopropyl)-trimethoxysilane [APTMS] was used as a precursor to form the SiO_x shell layer in a pH value of 4–5.

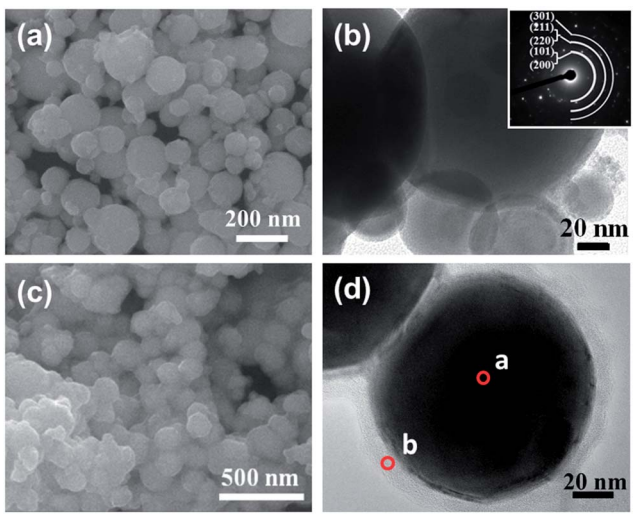

Fig. 3 (a) SEM and (b) TEM images of pure Sn NPs. The inset in (b) shows the corresponding selected area diffraction patterns, for which each plane has been indexed. (c) SEM and (d) TEM images of Sn/SiO_x core–shell NPs. The corresponding SEM image is shown in the inset.

approximately 10 nm-thick SiO_x layer formed on the surface of Sn NPs. The composition of the Sn/SiO_x core–shell NPs was further examined by the energy dispersive X-ray spectroscopy (EDS) analysis. The EDS results shown in Table S1† confirm the configuration of the inner Sn core and the outer SiO_x shell for the as-prepared NPs. The core–shell configuration was further highlighted by a high annular angle dark field (HAADF) image shown in Fig. S3† where a dark shell layer surrounding the bright inner core was observed. The observed image contrast in the HAADF image is a result of the dissimilar electron scattering behaviors in different materials. The Sn atom has a higher atomic number than the SiO_x layer, thereby resulting in the image contrast.

The thermal stability of the Sn/SiO_x core–shell NPs was examined by *in situ* heating X-ray diffraction (XRD) with continuous thermal cyclic measurements from room temperature (RT) to 250 °C to RT, as shown in Fig. 4. At RT, peaks in XRD spectra indicate the phase of the pure Sn [JCPD number: 86-2265] whereas no peak related to SiO_x can be found at RT because of its amorphous configuration. After increasing the temperature from RT to 100 °C, the intensity of peaks slightly increases as a result of the enhanced crystallization of the inner Sn NPs during thermal annealing. As the heating temperature increases to ~200 °C, approaching the melting point of Sn, the inner Sn NPs gradually turn into a molten state. As a result, Sn crystalline peaks disappear. The same phenomenon was observed when the temperature increases to 250 °C. During the cooling process, the Sn crystalline peaks appear again as the temperature decreases to 100 °C. This indicates that the Sn content inside the NPs recrystallizes during the cooling process and the Sn NPs are well-protected by the SiO_x shells. For comparison, the thermal stability of pure Sn NPs post-thermally treated with rapid thermal annealing at 100 °C, 150 °C, and 200 °C, respectively, was examined, as shown in Fig. S4† (heat rate: 20 °C s^{-1}; duration time for 5 min). XRD spectra for the pure Sn NPs are also provided in Fig. S4† for comparison. It was found that there is no apparent change in XRD spectra for 100 °C-treated Sn NPs. However, SnO peaks were found for 150 °C-treated Sn NPs, presumably due to a lack of the SiO_x protection layer. As the annealing temperature increases to 200 °C, the oxidation of Sn NPs into SnO_2 occurs.

Note that the thickness of the SiO_x shell layer plays an important role in the stability of the Sn/SiO_x core–shell NPs during the thermal cycle test. We found that if the thickness of the SiO_x layer is below ~5 nm, the oxidation process, namely

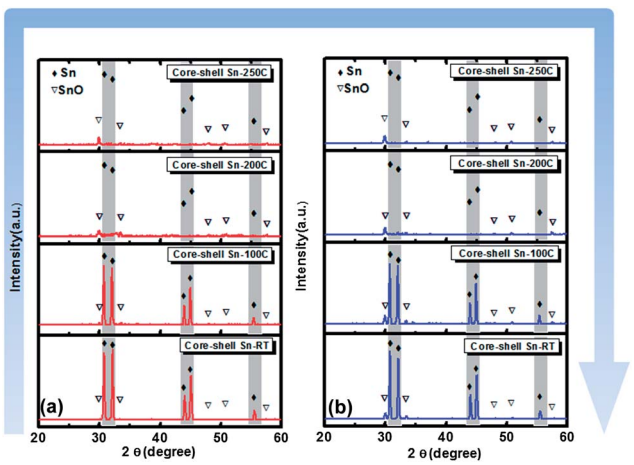

Fig. 4 *In situ* XRD results show a reversible heating cycle for Sn/SiO_x core–shell NPs.

formation of the SnO or SnO_2 phase, occurs. It is worthy to note that the 10 nm-thick SiO_x shell layer adopted in the present study can prevent the oxidation process at a heating temperature of 500 °C. This is suitable to fit the working range of the current molten salt. To demonstrate that the as-prepared Sn/SiO_x core–shell NPs are applicable for operation at high temperature, the as-prepared core–shell NPs underwent 500 °C-RTA treatment. The XRD spectra of 500 °C thermally treated core–shell NPs and as-prepared core–shell NPs are shown in Fig. S5.† No difference in XRD patterns from the two samples can be found. This confirms that the SiO_x shell layer can efficiently protect the pure-Sn cores from being oxidized during the high temperature operation.

The latent heat of the Sn and Sn/SiO_x core–shell NPs was examined using the differential scanning calorimetry measurements (DSC, DSC1 from Mettler–Toledo). In Fig. 5(a), the solid, dot, and dash-point lines represent the results from three consecutive measurements for the Sn/SiO_x core–shell NPs, whereas the inset in Fig. 5(a) shows the corresponding results for Sn NPs without the preservation of an oxide layer. The latent heat absorption was evaluated from the area of the valley on the heat flow profile at approximately 225 °C,[18] which gives a latent heat of approximately 29 J g^{-1} and 45 J g^{-1} for Sn/SiO_x and Sn NPs, respectively. The obtained latent heat values are smaller than the value of 58 J g^{-1} for bulk Sn, which is mainly the result of the spontaneous formation of a thin SnO layer at RT (see Fig. 3(c)) and the following oxidation during the heating process in DSC measurements. In addition, the large reduction of the latent heat for the core–shell Sn/SiO_x NPs is due to an overestimated weight in evaluating the latent heat in DSC measurements. The weight used in evaluating the latent heat for core–shell NPs includes the portion of the SiO_x shell, while the latent heat is only contributed from the core portion of the NPs. Fig. 5(b) shows the results for consecutive measurements for the latent heat of Sn and Sn/SiO_x core–shell NPs, respectively. Obviously, Sn/SiO_x core–shell NPs exhibit a stable latent heat of approximately 29 J g^{-1}. On the other hand, the latent heat of pure Sn NPs decreases with repeating measurements because of the continuous oxidation of Sn NPs. This suggests that our synthesized core–shell NPs are suitable for practical applications. The latent heat of the Sn NPs saturates to approximately 15 J g^{-1} because of the formation of a thick tin oxide layer. The thick oxide layer prohibits further oxidation of Sn NPs. Furthermore, the Sn/SiO_x core–shell NPs were doped with the HITEC solar salt to investigate the effectiveness of the core–shell NPs in enhancing energy storage for solar-thermal power generation. The heat capacities for the pure HITEC salt and the HITEC salts doped with 1, 3, and 5 wt% Sn/SiO_x core–shell NPs are shown in Fig. 5(c). The obtained temperature-average HC of 1.57 J g^{-1} K^{-1} for the pure HITEC salt is

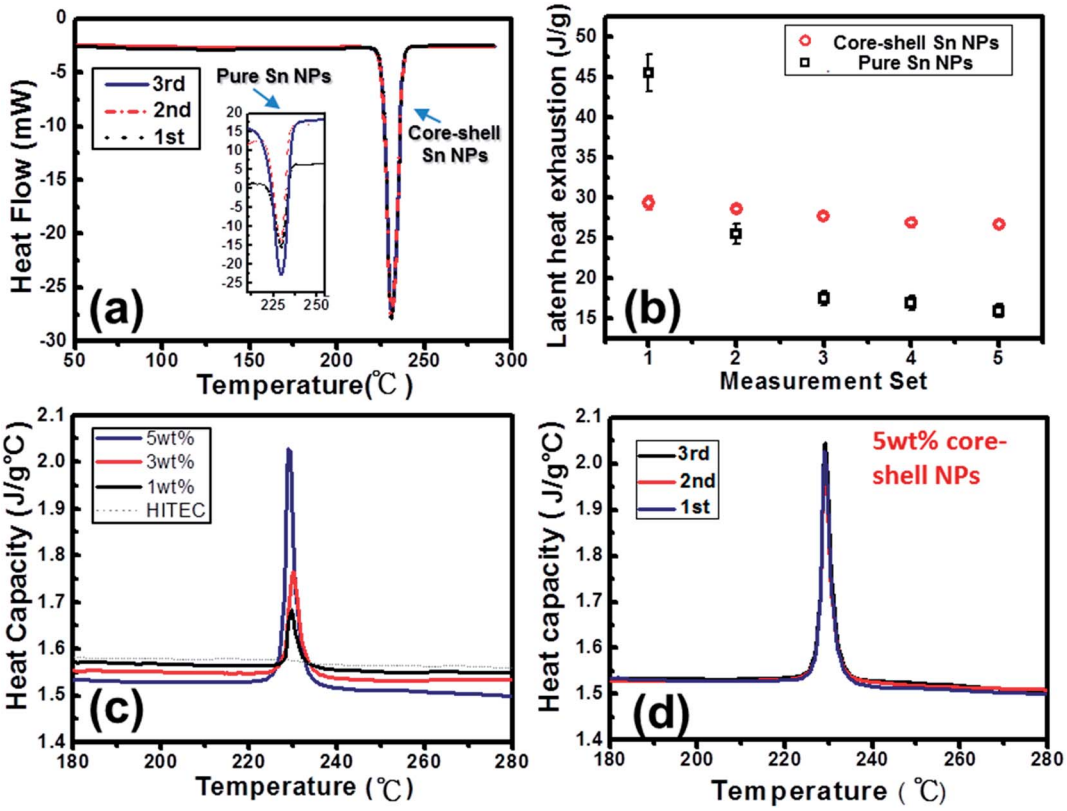

Fig. 5 (a) DSC curves of Sn/SiO_x core–shell and pure Sn NPs. (b) Latent heat exhaustion of pure Sn and Sn/SiO_x core–shell NPs at continuous thermal cycles. (c) HC measurements of the HITEC salt mixed with different concentrations of Sn/SiO_x NPs from 1, 3, and 5 wt% at different heating temperatures. (d) The endurance of HC tests for the HITEC salt mixed with 5 wt% Sn/SiO_x core–shell NPs. An enhanced HC of ~2.03 J g^{-1} K^{-1} was measured.

consistent with the literature report.[14] This average also validates our measurements. The enhancement of HCs of the salts doped with NPs is observed at the melting point of Sn NPs. The HCs for the salt doped with 1, 3, and 5 wt% core–shell Sn/SiO_x NPs can be enhanced to 1.67 J g^{-1} K^{-1}, 1.77 J g^{-1} K^{-1}, and 2.03 J g^{-1} K^{-1}, respectively, at the melting point. The release of the latent heat from Sn NPs is responsible for the enhancement of HCs at the melting point despite the inherently different heat capacities of the Sn NPs and the HITEC salt. Fig. 5(d) shows the corresponding endurance test of the HITEC solar salt doped with 5 wt% Sn/SiO_x core–shell NPs. The results indicate that the 5 wt% NP doped HITEC solar salt exhibits a stable enhancement of capacity of 2.03 J g^{-1} K^{-1} at the melting point. The morphology of the 5 wt% core–shell NP doped HITEC solar salt is shown in Fig. S6,† where the Sn/SiO_x core–shell NPs are uniformly dispersed in the HITEC salt matrix.

An increased HC can be theoretically achievable *via* increasing the concentration of NPs in the HITEC salt. However, the increased particle concentration will also result in an increased fluid viscosity, thereby impeding the efficiency of the power plant.[19] To overcome this dilemma, the core material can be replaced by binary, ternary alloys with higher latent heat to obtain a HC enhancement in a certain temperature range which leaves the viscosity unaffected.

3. Conclusion

We have demonstrated stable Sn/SiO_x core–shell NPs for the enhancement of energy storage for solar-thermal power generation. The stable Sn/SiO_x NPs during the thermal heating and cooling cycles were investigated by *in situ* heating XRD to provide dynamic information about solidification and melting behaviors. The latent heat of ~29 J g^{-1} for the Sn/SiO_x core–shell NPs was measured and the enhanced heat capacity was achieved from 1.57 to 2.03 J g^{-1} K^{-1} for the HITEC molten without and with a mixture of 5% Sn/SiO_x core–shell NPs. Endurance cycle testing further proves the stable operation of the doped salt in a real practical application. The concept in this study can be applied to enhance energy storage in solar-thermal power generation.

Acknowledgements

The research was supported by the National Science Council through Grant no. NSC 101-2112-M-007-015-MY3, 102-2633-M-007-002, 101-2221-E-007-090-MY3, and the National Tsing Hua University through Grant no. 102N2022E1. C. C. Lai thanks the members in Nanoscience and Nanodevices Lab, NTHU, for experimental discussion. Y. L. Chueh greatly appreciates the use of the facility at CNMM, National Tsing Hua University through Grant no. 102N2744E1.

References

1 C. Lueken, G. E. Cohen and J. Apt, Costs of solar and wind power variability for reducing CO_2 Emissions, *Environ. Sci. Technol.*, 2012, **46**(17), 9761.
2 B. Dursuna and G. C. Cihan, The role of hydroelectric power and contribution of small hydropower plants for sustainable development in Turkey, *Renewable Energy*, 2011, **36**(4), 1227.
3 M. Z. Jacobsona and M. A. Delucchib, Providing all global energy with wind, water, and solar power, part I: Technologies, energy resources, quantities and areas of infrastructure, and materials, *Energy Policy*, 2011, **39**(3), 1154.
4 S. Rahman, Green power: What is it and where can we find it?, *Power and Energy Magazine, IEEE*, 2003, **1**(1), 30.
5 J. Oh, H. C. Yuan and H. M. Branz, An 18.2%-efficient black-silicon solar cell achieved through control of carrier recombination in nanostructures, *Nat. Nanotechnol.*, 2012, **7**(11), 743.
6 P. Grimaldi and I. Grimaldi, *Solar Tres: Proposal of a solar-only 24-hour-operation Solar Tower Plant for Southern Spain Solar Thermal*, Sydney, Australia, 2000.
7 M. Medrano, A. Gil, I. Martorell, X. Potau and L. F. Cabeza, State of the art on high-temperature thermal energy storage for power generation. part 2—case studies, *Renewable Sustainable Energy Rev.*, 2010, **14**(1), 56.
8 S. D. Sharma and K. Sagara, Latent Heat Storage Materials and Systems: A Review, *Int. J. Green Energy*, 2005, **2**, 1.
9 E. Sauer, *Energietransport-speicherung und verteilung. TechnischerVerlagResch*, Verlag T Ü V Rheinland, Koln, Germany, 1982.
10 R. Velraj, R. V. Seeniraj, R. Hafner, C. Faber and K. Schwarzer, Heat transfer enhancement in a latent heat storage system, *Sol. Energy*, 1999, **65**, 171.
11 M. M. Farid, A. M. Khudhair, S. A. Razack and S. Al-Hallaj, A review on phase change energy storage: materials and applications, *Energy Convers. Manage*, 2004, **45**, 1597.
12 W. D. Steinmann and R. Tamme, Latent heat storage for solar steam systems, *J. Sol. Energy Eng.*, 2008, **130**, 11004.
13 M. N. A. Hawlader, M. S. Uddin and M. M. Khin, Microencapsulated PCM thermal-energy storage system, *Appl. Energy*, 2003, **74**, 195.
14 U. S. Choi, *Enhancing thermal conductivity of fluids with nanoparticles*, ASME Fed., 1995, vol. 231, p. 99.
15 HITEC Solar Salt, Technical Bulletin, Coastal Chemical Co., LLC.
16 T. Ung, L. M. Liz-Marzán and P. Mulvaney, Controlled method for silica coating of silver colloids. Influence of coating on the rate of chemical reactions, *Langmuir*, 1998, **14**(14), 3740.
17 Y. Kobayashi, H. Katakami, E. Mine, D. Nagao, M. Konno and L. M. Liz-Marzán, Silica coating of silver nanoparticles using a modified Stöber method, *J. Colloid Interface Sci.*, 2005, **283**(2), 392.
18 D. Banu, D. Feldman and D. Hawes, Evaluation of thermal storage as latent heat in phase change material wallboard by differential scanning calorimetry and large scale thermal testing, *Thermochim. Acta*, 1998, **317**(1), 39–45.
19 S. M. S. Murshed, K. C. Leong and C. Yang, Investigations of thermal conductivity and viscosity of nanofluids, *Int. J. Therm. Sci.*, 2008, **47**, 560.